Coupling the BEM/TBEM and the MFS for the numerical simulation of acoustic wave propagation and transient conduction heat transfer

A. Tadeu[1], J. António[1], N. Simões[1], I. Simões[2] & I. Castro[2]
[1]*CICC, Department of Civil Engineering, University of Coimbra, Portugal*
[2]*ITeCons, Coimbra, Portugal*

Abstract

The coupling of the Boundary Element Method (BEM) / the Traction Boundary Element Method (TBEM) and the Method of Fundamental Solutions (MFS) is proposed for the transient analysis of acoustic wave propagation problems and conduction heat transfer, thereby overcoming the limitations posed by each method. The full domain is divided into sub-domains which are modeled using the BEM/TBEM and the MFS, and the sub-domains are coupled with the imposition of the adequate boundary conditions.

The applicability of the proposed method is shown by simulating the acoustic behavior of a rigid acoustic screen in the vicinity of a dome and by simulating the thermal behavior of a solid ring incorporating a crack in its wall.

Keywords: coupling BEM, TBEM and MFS, wave propagation, heat diffusion.

1 Introduction

The Boundary Element Method (BEM) is one of the most suitable for modeling homogeneous unbounded systems containing irregular interfaces and inclusions since the far field conditions are automatically satisfied and only the boundaries of the interfaces and inclusions need to be discretized. Despite the fact that the BEM requires only boundary meshing it still needs prior knowledge of fundamental solutions, i.e., Green's functions. Its efficiency also depends on the correct integration of the singular and hypersingular integrals. In addition, for a certain level of accuracy, the number of boundary elements depends on the

WIT Transactions on Modelling and Simulation, Vol 50, © 2010 WIT Press
www.witpress.com, ISSN 1743-355X (on-line)
doi:10.2495/BE100231

excitation frequency, requiring the use of many boundary elements to model high frequency responses. This leads to an undesirably high computational cost.

Furthermore, the BEM tends to break down when applied to cracks and very thin heterogeneities [1]. The Traction Boundary Element Method (TBEM) is a numerical method that solves the thin-body difficulties that arise when modeling wave propagation in the presence of very thin heterogeneities such as small imperfections, dimensionless cracks or almost imperceptible defects. Different attempts have been made to overcome this difficulty [2, 3]. Most of the work published refers to the cases of 2D and, in some cases, 3D geometries. Amado Mendes and Tadeu [4] solved the case of a 2D empty crack buried in an unbounded medium subjected to a 3D source. The solution requires the application of a spatial Fourier transform along the direction in which the geometry of the crack does not vary. Thus, the 3D solution is obtained as a summation of 2D solutions for different spatial wavenumbers. The resulting hypersingular kernels were computed analytically by defining the dynamic equilibrium of semi-cylinders above the boundary elements that discretize the crack. Following that, Tadeu et al. [5] proposed a combined (or dual) BEM/TBEM formulation able to solve the case of fluid-filled thin inclusions placed in an unbounded medium, and in [6] they applied the same numerical techniques to the case of elastic scattering produced by thin rigid inclusions.

In recent years, a different class of numerical techniques has become popular recently: the so-called meshless techniques that require neither domain nor boundary discretization [7–9]. The method of fundamental solutions (MFS) seems to be particularly effective for studying wave propagation since it overcomes some of the mathematical complexity of the BEM and provides acceptable solutions at substantially lower computational cost. Godinho et al. [10] studied the performance of the MFS for simulating the propagation of acoustic waves in a fluid domain with an inclusion. The authors concluded that the method can be very efficient, even outperforming the BEM for this type of problem. Godinho et al. [11] subsequently successfully employed the MFS to study acoustic and elastic wave propagation around thin structures using a domain decomposition technique. Still, the use of the MFS has its own shortcomings and limitations in the presence of thin inclusions and inclusions with twisting (sinuous) boundaries.

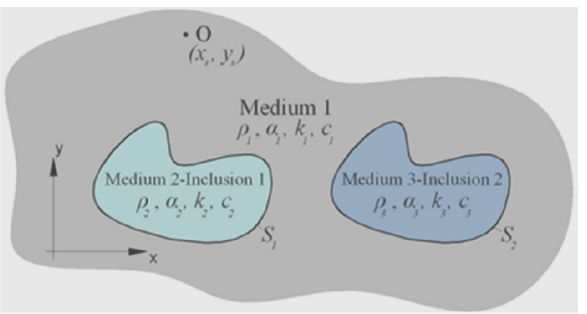

Figure 1: Sketch representing the geometry of the problem.

This paper describes the coupling of the BEM/TBEM and the MFS to overcome some of the limitations posed separately by each method. These coupling formulations are presented for the transient analysis of acoustic wave propagation and heat diffusion problems in the presence of null-thickness and thin inclusions. The applicability of the proposed method is shown by means of two numerical examples.

2 Problem definition

2.1 Acoustic wave propagation

Consider two 2D irregular cylindrical inclusions, submerged in a spatially uniform fluid medium 1 with density ρ_1 (Figure 1). This system is subjected to a harmonic line pressure source at $\mathrm{O}(x_s, y_s)$, which oscillates with a frequency ω, and originates an incident pressure at (x, y),

$$p_{inc}(x, y, \omega) = AH_0(k_{\alpha_1} r_1) \tag{1}$$

where the subscript inc represents the incident field, $r_1 = \sqrt{(x - x_s)^2 + (y - y_s)^2}$, A the wave amplitude, $k_{\alpha_1} = \dfrac{\omega}{\alpha_1}$, α_1 the pressure wave velocity of the fluid medium, and $H_n(\ldots)$ correspond to second Hankel functions of order n. The fluid media 2 and 3 inside inclusions 1 and 2 have densities ρ_2 and ρ_3 and allow pressure wave velocities α_2 and α_3, respectively.

For frequency domain analysis, the pressure (p) can be calculated using the Helmoltz equation:

$$\left(\frac{\partial^2}{\partial x^2} + \frac{\partial^2}{\partial y^2}\right) p(x, y, \omega) + (k_\alpha)^2 p(x, y, \omega) = 0 \tag{2}$$

2.2 Transient conduction heat transfer

Consider the two irregular 2D cylindrical inclusions, 1 and 2, embedded in a spatially uniform solid medium (Medium 1) with thermal diffusivity K_1 (as in Figure 1). Media 2 and 3, inside inclusions 1 and 2, exhibit thermal diffusivities K_2 and K_3, respectively. Thermal diffusivity K_j is defined by $\dfrac{k_j}{\rho_j c_j}$, where k_j is the thermal conductivity, ρ_j is the density and c_j is the specific heat of each Medium j. Consider further that this system is subjected a line heat source placed at $\mathrm{O}(x_s, y_s)$.

The transient heat transfer by conduction in each homogeneous and isotropic medium can be described by the diffusion equation in Cartesian coordinates, in the frequency domain,

$$\left(\frac{\partial^2}{\partial x^2}+\frac{\partial^2}{\partial y^2}\right)T(x,y,\omega)+\left(\sqrt{\frac{-\mathrm{i}\omega}{K_j}}\right)^2\nabla^2 T(x,y,\omega)=0 \tag{3}$$

In the frequency domain the incident heat diffusion generated at (x,y) can be expressed by

$$t_{inc}(x,y,\omega)=\frac{-\mathrm{i}\,A}{4k_1}H_0\left(\sqrt{-\frac{\mathrm{i}\omega}{K_1}}r_1\right) \tag{4}$$

3 Boundary integral coupling formulations

3.1 BEM/MFS coupling formulation

Considering the inclusion 1, bounded by a surface S_1, and subjected to an incident pressure (p_{inc})/heat field (t_{inc}) given by u_{inc} the following boundary integral equation can be constructed:

a) Along the exterior domain of inclusion 1 (Medium 1)

$$\begin{aligned} c\,u^{(1)}(x_0,y_0,\omega) = &\int_{S_1} q^{(1)}(x,y,n_{n1},\omega)\,G^{(1)}(x,y,x_0,y_0,\omega)\,ds - \\ &\int_{S_1} H^{(1)}(x,y,n_{n1},x_0,y_0,\omega)\,u^{(1)}(x,y,\omega)\,ds + u_{inc}(x_0,y_0,x_s,y_s,\omega) \end{aligned} \tag{5}$$

In these equations, the superscript 1 corresponds to the exterior domain; n_{n1} is the unit outward normal along the boundary S_1; G and H are respectively the fundamental solutions (Green's functions) for the pressure/temperature (u) and pressure gradient/heat flux (q), at (x,y) due to a virtual load at (x_0,y_0). u_{inc} is the pressure/heat incident field at (x_0,y_0), when the point source is located at (x_s,y_s). The factor c is a constant defined by the shape of the boundary, taking the value $1/2$ if $(x_0,y_0)\in S_1$ and S_1 is smooth (otherwise c=0).

Equation (5) does not yet take into account the presence of the neighboring inclusion 2, which is modeled using the MFS. The MFS assumes that the response of this neighboring inclusion is found as a linear combination of fundamental solutions simulating the pressure/heat field generated by two sets of NS virtual sources. These virtual loads are distributed along the inclusion interface at distances δ from that boundary towards the interior and exterior of the inclusion (lines $\hat{C}^{(2)}$ and $\hat{C}^{(1)}$ in Figure 2) in order to avoid singularities. Sources inside the inclusion have unknown amplitudes $a^{(2)}_{n\_ext}$, while those placed outside the inclusion have unknown amplitudes $a^{(2)}_{n\_int}$. In the exterior and interior fluid medium, the reflected fields are given by

$$u^{(1)}(x,y,\omega) = \sum_{n\_ext=1}^{NS} \left[a^{(2)}_{n\_ext} G^{(1)}(x,y,x_{n\_ext}, y_{n\_ext}, \omega) \right]$$
$$u^{(3)}(x,y,\omega) = \sum_{n\_int=1}^{NS} \left[a^{(2)}_{n\_int} G^{(3)}(x,y,x_{n\_int}, y_{n\_int}, \omega) \right] \quad (6)$$

where $G^{(1)}$ and $G^{(3)}$ are the fundamental solutions which represent the pressures/temperatures at points (x,y) in mediums 1 and 3, generated by pressure/heat sources acting at positions (x_{n_ext}, y_{n_ext}) and (x_{n_int}, y_{n_int}). n_ext and n_int are the subscripts that denote the load order number placed along lines $\hat{C}^{(2)}$ and $\hat{C}^{(1)}$, respectively.

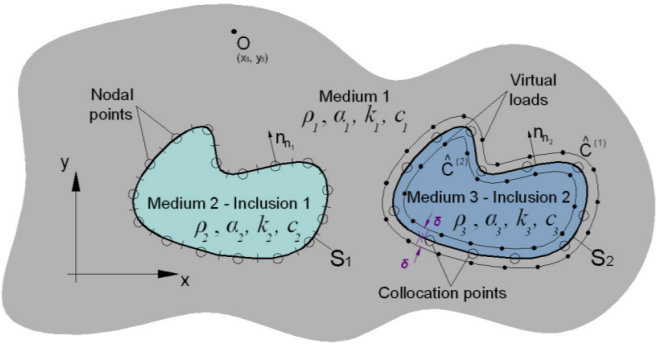

Figure 2: Discretization of the system: boundary elements, position of virtual loads and collocation points.

The pressure/heat field generated by this second inclusion can be viewed as an incident field that strikes the first inclusion. So eqn (5) needs to be modified accordingly,

$$c\,u^{(1)}(x_0,y_0,\omega) = \int_{S_1} q^{(1)}(x,y,n_{n1},\omega)\, G^{(1)}(x,y,x_0,y_0,\omega)\, ds$$
$$- \int_{S_1} H^{(1)}(x,y,n_{n1},x_0,y_0,\omega)\, u^{(1)}(x,y,\omega)\, ds + u_{inc}(x_0,y_0,x_s,y_s,\omega) \quad (7)$$
$$+ \sum_{n\_ext=1}^{NS} \left[a^{(2)}_{n\_ext} G^{(1)}(x,y,x_{n\_ext}, y_{n\_ext}, \omega) \right]$$

b) Along the interior domain of inclusion 1 (Medium 2)

$$c\,u^{(2)}(x_0,y_0,\omega) = \int_{S_1} q^{(2)}(x,y,n_{n1},\omega) G^{(2)}(x,y,x_0,y_0,\omega)\, ds - \int_{S_1} H^{(2)}(x,y,n_{n1},x_0,y_0,\omega) u^{(2)}(x,y,\omega)\, ds \quad (8)$$

In eqn (8), the superscript 2 corresponds to the domain inside inclusion 1.

c) Along the interior and exterior domain of inclusion 2 (Mediums 1 and 3)

To determine the amplitudes of the unknown virtual loads $a^{(2)}_{n\_ext}$ and $a^{(2)}_{n\_int}$, it is also necessary to impose the continuity of pressures/temperatures and normal

pressure gradients/heat fluxes at interface S_2, boundary of inclusion 2, along NS collocation points (x_{col}, y_{col}). This must be done taking into account the reflected field generated at inclusion 1. Thus the following two equations are defined,

$$\int_{S_1} q^{(1)}(x,y,n_{n1},\omega)\,G^{(1)}(x,y,x_{col},y_{col},\omega)\,ds - \int_{S_1} H^{(1)}(x,y,n_{n1},x_{col},y_{col},\omega)\,u^{(1)}(x,y,\omega)\,ds + u_{inc}(x_{col},y_{col},x_s,y_s,\omega) + \sum_{n\_ext=1}^{NS}\left[a^{(2)}_{n\_ext}\,G^{(1)}(x_{col},y_{col},x_{n\_ext},y_{n\_ext},\omega)\right] = \sum_{n\_int=1}^{NS}\left[a^{(2)}_{n\_int}\,G^{(3)}(x_{col},y_{col},x_{n\_int},y_{n\_int},\omega)\right] \tag{9}$$

$$\int_{S_1} q^{(1)}(x,y,n_{n1},\omega)\frac{\partial G^{(1)}}{\partial n_{n2}}(x,y,n_{n2},x_{col},y_{col},\omega)\,ds - \int_{S_1}\frac{\partial H^{(1)}}{\partial n_{n2}}(x,y,n_{n1},n_{n2},x_{col},y_{col},\omega)\,u^{(1)}(x,y,\omega)\,ds + \frac{\partial u_{inc}}{\partial n_{n2}}(x_{col},y_{col},n_{n2},x_s,y_s,\omega) + \sum_{n\_ext=1}^{NS}\left[a^{(2)}_{n\_ext}\frac{\partial G^{(1)}}{\partial n_{n2}}(x_{col},y_{col},n_{n2},x_{n\_ext},y_{n\_ext},\omega)\right] = \sum_{n\_int=1}^{NS}\left[a^{(2)}_{n\_int}\,\gamma\,\frac{\partial G^{(3)}}{\partial n_{n2}}(x_{col},y_{col},n_{n2},x_{n\_int},y_{n\_int},\omega)\right] \tag{10}$$

In these equations, n_{n2} is the unit outward normal along the boundary S_2, $\gamma = \dfrac{\rho_1}{\rho_3}$ in the acoustic wave propagation case and $\gamma = \dfrac{k_3}{k_1}$ for the heat transfer problem.

d) Final system of equations

The global solution is obtained by solving eqns (7)–(10). This requires the discretization of the interface S_1, boundary of inclusion 1 into N straight boundary elements (see Figure 2).

The required two-dimensional Green's functions for pressure and pressure gradients in Cartesian co-ordinates are those for an unbounded medium,

$$G^{(m)}(x,y,x_k,y_k,\omega) = \frac{\mathrm{i}}{4}H_0\left(k_{\alpha_m}\,r\right)$$
$$H^{(m)}(x,y,n_{n1},x_k,y_k,\omega) = \frac{-\mathrm{i}}{4}k_{\alpha_m}H_1\left(k_{\alpha_m}\,r\right)\frac{\partial r}{\partial n_{n1}} \tag{11}$$

in which $r = \sqrt{(x-x_k)^2 + (y-y_k)^2}$ and (x_k, y_k) correspond to the loaded point. The pressure wave velocities in these equations are the ones associated with the exterior and the interior fluid of the inclusions (m).

The required two-dimensional Green's functions for temperature and temperature gradients in Cartesian co-ordinates are,

$$G^{(m)}(x,y,x_k,y_k,\omega) = \frac{-i}{4}H_0\left(k_{\alpha_m}\,r\right)$$
$$H^{(m)}(x,y,n_{n1},x_k,y_k,\omega) = \frac{i}{4}k_{\alpha_m}H_1\left(k_{\alpha_m}\,r\right)\frac{\partial r}{\partial n_{n1}} \tag{12}$$

in which $k_{\alpha_m} = \sqrt{\dfrac{-\mathrm{i}\omega}{K_m}}$.

The final integral equations are manipulated and combined so as to impose the continuity of pressure/temperature and pressure gradients/heat fluxes along the boundary of the inclusions 1 and 2. The solution of this system of equations gives the nodal pressures/temperatures and pressure gradients/heat fluxes along the boundary S_1 and the unknown virtual load amplitudes, $a^{(2)}_{n\_ext}$ and $a^{(2)}_{n\_int}$, which allow the pressure/heat field to be defined inside and outside the inclusions.

In the case of null normal pressure gradients/ null heat fluxes or null pressures/temperatures along the inclusions boundaries, the eqns (14)–(17) can be simplified (not shown).

3.2 TBEM/MFS coupling formulation

The Traction Boundary Element Method (TBEM) can be formulated as for the case of thin inclusions (Tadeu et al. [12]), leading to the following eqns (13)–(14) that replace the former eqns (7)–(8), while modeling the first inclusion:

$$a\,u^{(1)}(x_0,y_0,\omega)+c\,q^{(1)}(x_0,y_0,n_{n1},\omega)=\int_{S_1} q^{(1)}(x,y,n_{n1},\omega)\,\overline{G}^{(1)}(x,y,n_{n2},x_0,y_0,\omega)\,ds$$
$$-\int_{S_1}\overline{H}^{(1)}(x,y,n_{n1},n_{n2},x_0,y_0,\omega)\,u^{(1)}(x,y,\omega)\,ds+\overline{u}_{inc}(x_0,y_0,n_{n2},x_s,y_s,\omega) \tag{13}$$
$$+\sum_{n\_ext=1}^{NS}\left[a^{(2)}_{n\_ext}\overline{G}^{(1)}(x,y,n_{n2},x_{n\_ext},y_{n\_ext},\omega)\right]$$

$$a\,u^{(2)}(x_0,y_0,\omega)+c\,q^{(2)}(x_0,y_0,n_{n1},\omega)$$
$$=\int_{S_1} q^{(2)}(x,y,n_{n1},\omega)\,\overline{G}^{(2)}(x,y,n_{n2},x_0,y_0,\omega)\,ds\int_{S_1}\overline{H}^{(2)}(x,y,n_{n1},n_{n2},x_0,y_0,\omega)\,u^{(2)}(x,y,\omega)\,ds \tag{14}$$

Eqns (9)–(10) can be kept the same.

The required two-dimensional Green's functions, $\overline{G}^{(m)}(x,y,n_k,x_k,y_k,\omega)$ and $\overline{H}^{(m)}(x,y,n_n,n_k,x_k,y_k,\omega)$ are defined by mathematical manipulation of eqns (11), (12), while $\overline{u}_{inc}(x,y,n_k,x_s,y_s,\omega)$ is obtained from eqns (1), (4), where n_k and n_n are the unit outward normal for the boundary segments being loaded and integrated, respectively.

4 Verification of the coupling algorithms

The proposed coupling algorithms (BEM/MFS, TBEM/MFS and combined BEM+TBEM/MFS) described have been verified against BEM and MFS solutions (not shown). Analysis of the results reveals a very good agreement between the proposed coupling solutions and both the BEM and MFS models' solutions for both cases, wave acoustic propagation and heat transfer problems.

5 Applications

The applicability of the proposed coupling formulations is illustrated by solving two problems. The acoustic behavior of a rigid acoustic screen in the vicinity of

a dome is addressed in the first example. The second example concerns the computation of the thermal field produced by a heat source in a ring system filled with solid material, incorporating defects in its wall.

Given that the computations are performed in the frequency domain, time responses in the space domain are computed by applying an inverse (Fast) Fourier Transform in ω .

It is essential that $\Delta\omega$ is small enough to avoid contaminating the response in the time domain (aliasing phenomena). This is almost eliminated by the introduction of complex frequencies with a small imaginary part of the form $\omega_c = \omega - i\eta$ (with $\eta = 0.7\Delta\omega$).

5.1 Acoustic application - null-thickness rigid acoustic screen in the vicinity of a dome

A rigid acoustic screen, placed in a vicinity of a dome, is used to illustrate the capabilities of the proposed TBEM/MFS formulation. The pressure source is placed 4.0 m from the barrier in the horizontal direction, and 0.5 m above the ground, as Figure 3 shows. The barrier, 3.0 m tall, is placed 5.0 m from a semi-circular dome.

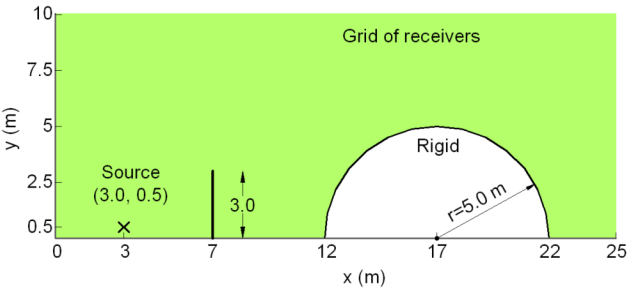

Figure 3: Geometry of the rigid acoustic screen in the vicinity of a dome and position of the source and grid of receivers.

The wave velocity allowed in the host medium and its density are kept constant and equal to 340 m/s and 1.29 kg/m^3, respectively.

The computations are performed in the frequency domain for frequencies ranging from 4 Hz to 2048 Hz, with a frequency increment of 4 Hz, which determines a total time window for the analysis of 0.25 s.

The pressure response is obtained over a two-dimensional grid of 26347 receivers arranged along the x and y directions at equal intervals and placed in the vicinity of the acoustic barrier and dome from $x = 0.0$m to $x = 25.0$m and from $y = 0.0$m to $y = 10.0$m.

The barrier is modeled as a rigid screen using the TBEM. It has null-thickness and is discretized using an appropriate number of boundary elements defined by the relation between the wavelength and the length of the boundary elements, which was set at 6. A minimum of 30 boundary elements were used. The dome is

assumed to be rigid and simulated by MFS, using a minimum of 200 virtual loads/collocation points. The virtual loads are placed 0.5 m from its boundary. This number increases with the frequency according to the relation between the wavelength and the distance between collocation points, which was set at 6.

The source time dependence is assumed to be a Ricker wavelet with a characteristic frequency of 500 Hz. A set of snapshots taken from computer animations is presented to illustrate the resulting wave field in the vicinity of both the acoustic barrier and dome at different time instants.

The system is subjected to a pressure pulse, with a characteristic frequency of 500.0Hz, which starts acting at $t = 0$ s. Figure 4: shows contour plots of the pressure field at different time instants when the waves propagate in the vicinity of the acoustic barrier. In the plots, red represents the higher pressure amplitudes and blue the lower ones.

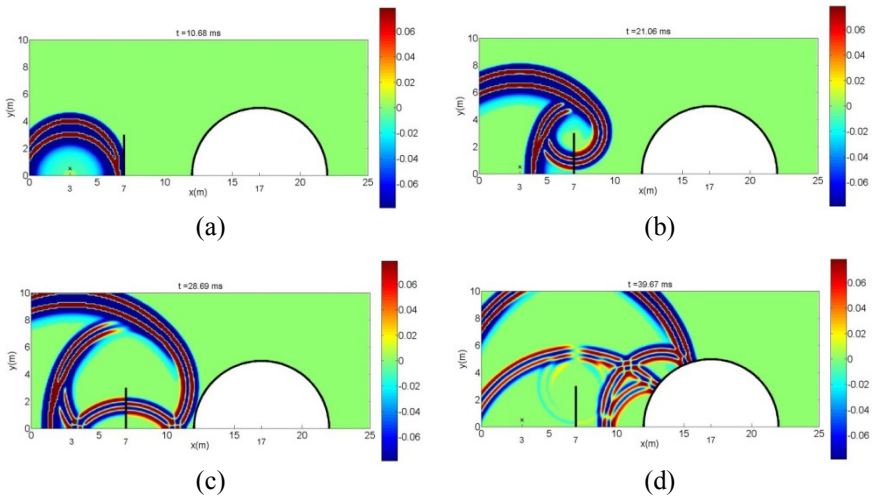

Figure 4: Pressure wave propagation in the vicinity of an acoustic barrier and a dome. Time responses at t = 10.68 ms (a), t = 21.06 ms (b), t = 28.69 ms (c) and t = 39.57 (d).

At t = 10.68 ms the incident pulse has just hit the acoustic barrier. The reflected pulse is still very close to the acoustic barrier. At t = 21.06 ms the diffracted waves that originate at the top of the barrier can be seen traveling around the screen. At t = 28.69 ms these waves are reflected on the ground, travelling upwards. As time passes the first set of reflections from the dome are visible (t = 39.67 ms).

5.2 Heat transfer application - null-thickness crack placed in the ring's wall

A null-thickness crack is placed in the wall as shown in Figure 5(b). The ring's wall is made of concrete ($k = 1.40$ W.m^{-1}.ºC^{-1}, ρ=2300.0 kg.m^{-3}, $c = 880.0$J.kg^{-1}.ºC^{-1}),

the solid filling the ring is steel ($k = 52.9$ W.m^{-1}.ºC^{-1}, ρ=7640.0 kg.m^{-3}, $c = 486.0$J.kg^{-1}.ºC^{-1}) and the hosting fluid medium is air ($k = 0.026$ W.m^{-1}.ºC^{-1}, ρ=1.29 kg.m^{-3}, $c = 1000.0$J.kg^{-1}.ºC^{-1}). The inner diameter of the ring is 0.3 m and the wall thickness is 0.2 m (see Figure 5). The crack is placed in the middle of the ring's wall, forming a circular concentric arc of 45.0^o with a radius of 0.4 m. This system is subjected to a heat line source placed in the steel medium at point O $(0, 0)$. The source time dependence is assumed to be parabolic (see Figure 5(b)).

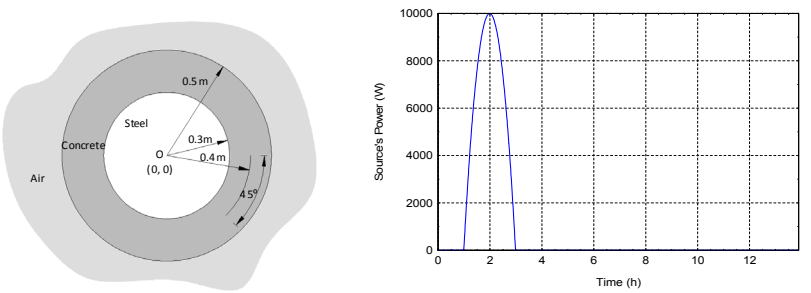

(a) (b)

Figure 5: Heat transfer problem: (a) Geometry of the cross-section of the ring containing a null-thickness crack. (b) Heat source power time evolution.

The computations are performed in the frequency domain for frequencies ranging from 0.0 Hz to 0.01026 Hz, with a frequency increment of 0.2×10^{-4} Hz (time window is 13.89 h).

The crack is modeled imposing null heat flux along its surface. The null-thickness crack is discretized using 28 boundary elements. In this example the TBEM model is used to simulate the thermal behavior of the crack for which the MFS would be less efficient. The other interface surfaces are simulated using the MFS that allows a better performance of the global model, without loss of accuracy. The inner and outer surfaces of the ring are modelled using a set of virtual heat sources placed at 0.05 m from the outer boundary and 0.03 m from inner boundary. The inner and the outer interfaces of the ring were modelled using 169 and 452 virtual and collocation points, respectively, evenly distributed.

The temperature distribution is obtained in a very fine two-dimensional grid of 1821 receivers equally spaced along the inner solid, wall and outer hosting fluid.

Figure 6 shows the temperature field at different time instants. To allow a better interpretation of the results presents the logarithm of the temperature results. In the first plot, at $t = 1.46$ h (Figure 6(a)), after the heat source has started emitting energy, a circular heat field can be observed in the host medium

caused by the energy propagation away from the heat source point. The incident heat pulse is visible propagating away from the source point without perturbations as it has not yet reached the wall of the ring. As expected, the amplitude of the temperature is uniform along the cylindrical heat wavefronts.

The presence of the crack causes a perturbation of the heat transfer along the cross-section of the wall. As time passes, the heat spreads around the crack. However, the receivers placed in the ring's wall, behind the crack, register considerably lower temperatures than the receivers placed on the other side, as can be seen at time $t = 7.93$ h (Figure 6(b)). Although the source power has already dropped to 0.0 W at $t = 3$ h, it is interesting to note that the temperature is still rising in some regions of the domain. This means that the energy introduced at the source point continues to propagate to colder regions in order to establish the equilibrium condition.

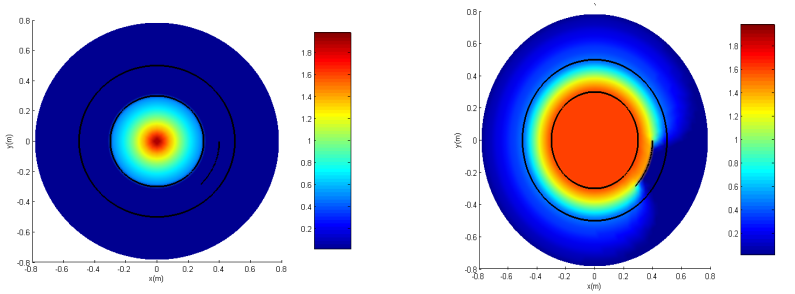

(a) (b)

Figure 6: Temperature distribution in the vicinity of a null-thickness crack with null heat fluxes prescribed along its surface, heated by a cylindrical line source. Time responses at $t = 1.46$ h (a) and $t = 7.93$ h (b).

6 Conclusions

The coupling between Boundary Element Method (BEM)/ Traction Boundary Element Method (TBEM) and the Method of Fundamental Solutions (MFS) has been proposed for the transient analysis of acoustic wave propagation and heat diffusion problems in the presence of multi-inclusions. It was demonstrated that the proposed coupling algorithms overcome limitations posed by each method. They require less computational power while maintaining adequate accuracy.

The TBEM coupled with the MFS, was proposed to overcome the thin-body difficulty. The proposed coupling formulations were used to solve two numerical examples. The propagation of two-dimensional pressure waves in the vicinity of a dome when a null-thickness rigid acoustic screen is placed between this structure and an acoustic source was addressed in the first example. The second example dealt with heat transient diffusion across a solid filled ring generated by a heat source, when an empty null-thickness crack is buried in the ring wall.

Acknowledgements

The research work presented herein was supported by the Portuguese Foundation for Science and Technology (FCT), under the research projects SFRH/BD/37425/2007 and SFRH/BD/48138/2008.

References

[1] Dell'erba, D.N., Aliabadi M.H. & Rooke D.P. *Dual boundary element method for three-dimensional thermoelastic crack problems*. Int. J. Fract; **94**, pp. 89–101, 1998.
[2] Rudolphi, T.J. *The use of simple solutions in the regularisation of hypersingular boundary integral equations.* Math. Comp. Modelling, **15**, pp. 269-278, 1991.
[3] Watson, J.O. *Singular boundary elements for the analysis of cracks in plane strain.* I. J. Num. Meths. Engg., **38**, pp. 2389-2411, 1995.
[4] Amado Mendes, P. & Tadeu, A. *Wave propagation in the presence of empty cracks in an elastic medium*, Computational Mechanics, Springer, **38(3)**, pp. 183-199, 2006.
[5] Tadeu, A., Amado Mendes, P. & António, J. *3D elastic wave propagation modelling in the presence of 2D fluid-filled thin inclusions*, Engineering Analysis with Boundary Elements (Special Issue "Non-Traditional Boundary Integral Formulations, Part II"), Elsevier, **30(3)**, pp. 176-193, 2006. (doi:10.1016/j.enganabound.2005.08.014).
[6] Tadeu, A., Amado Mendes, P. & António, J. *The simulation of 3D elastic scattering produced by thin rigid inclusions using the traction boundary element method*, Computers and Structures, Elsevier, **84(31-32)**, pp. 2244-2253, 2006. (doi:10.1016/j.compstruc.2006.08.034).
[7] Fairweather G., Karageorghis A. & Martin P.A. *The method of fundamental solutions for scattering and radiation problems.* Eng Anal Boundary Elem, **27**, pp. 759–69, 2003.
[8] Chen, J.T., Chang , M.H., Chen, K.H. & Chen, I.L.. *Boundary collocation method for acoustic eigenanalysis of three-dimensional cavities using radial basis function.* Comput Mech, **29**, pp. 392–408, 2002.
[9] Brown, D., Ling, L., Kansa, E. & Levesley, J. *On approximate cardinal preconditioning methods for solving PDEs with radial basis functions*. Eng Anal Boundary Elem, **29**, pp. 343–53, 2005;.
[10] Godinho, L., Tadeu, A. & Simões, N.A. *Accuracy of the MFS and BEM on the analysis of acoustic wave propagation and heat conduction problems*, Advances in Meshless Methods, Sladek Jan and Sladek Vladimir (Editors), Tech Science Press, 2006.
[11] Godinho, L., Tadeu, A. & Amado Mendes, P. *Wave propagation around thin structures using the MFS*, Comput. Mat. Contin., **5**, pp. 117–128, 2007.
[12] Tadeu, A., Amado Mendes, P. & António, J. *3D elastic wave propagation modelling in the presence of 2D fluid-filled thin inclusions*, Engineering Analysis with Boundary Elements (Special Issue "Non-Traditional Boundary Integral Formulations, Part II"), **30(3)**, pp. 176-193, 2006.